Journal of Power Sources 202 (2012) 230–235

Contents lists available at SciVerse ScienceDirect

Journal of Power Sources

journal homepage: www.elsevier.com/locate/jpowsour

Co_3O_4 nanorods/graphene nanosheets nanocomposites for lithium ion batteries with improved reversible capacity and cycle stability

Liqi Tao [a], Jiantao Zai [a], Kaixue Wang [a], Haojie Zhang [a], Miao Xu [a], Jie Shen [a], Yuezeng Su [b], Xuefeng Qian [a,*]

[a] School of Chemistry and Chemical Engineering and State Key Laboratory of Metal Matrix Composites, Shanghai Jiao Tong University, Shanghai 200240, PR China
[b] School of Aeronautics and Astronautics, Shanghai Jiao Tong University, Shanghai 200240, PR China

ARTICLE INFO

Article history:
Received 16 June 2011
Received in revised form 21 October 2011
Accepted 27 October 2011
Available online 22 November 2011

Keywords:
Cobalt oxide
Graphene nanosheets
Nanocomposite
Lithium ion batteries
Anode materials

ABSTRACT

Co_3O_4 nanorods/GNS (graphene nanosheets) nanocomposites have been synthesized through a one-spot solvothermal method, and characterized by X-ray diffraction, field emission scanning electron microscopy and transmission electron microscopy. Electrochemical performances reveal that the obtained Co_3O_4 nanorods/GNS nanocomposites exhibit improved cycling stability, remarkably high reversible lithium storage capacity and superior rate capability, e.g. approximate 1310 mAh g^{-1} and 1090 mAh g^{-1} of capacity are retained even after 40 cycles at a current density of 100 mA g^{-1} and 1000 mA g^{-1}, respectively. The high electrochemical performances can be attributed to the unique structure of Co_3O_4 nanorods/GNS nanocomposites, in which the 1D structure of Co_3O_4 can prevent the aggregation of Co_3O_4 and reduce the stacking degree of GNS, providing an excellent ion diffusion and electronic conduction pathway.

1. Introduction

Recently, lithium ion batteries (LIBs) have attracted extensive attention due to their high voltage, high specific energy and long working life [1–5]. Metal oxides, e.g. Fe_2O_3 [6], Co_3O_4 [7,8], NiO [9], MnO_2 [10], TiO_2 [11] and SnO_2 [12,13], are promising anode materials for LIBs because of their better electrochemical performance. Among these metal oxides, Co_3O_4 exhibits high specific capacity [7,8]. However, Co_3O_4 anode materials always suffer from rapid capacity fading because of the large volume expansion occurring during cycling process, which restricts their general applications. Thus, it is highly desirable to prepare Co_3O_4-based anode materials with improved electrochemical performance.

Graphene nanosheet (GNS) is a kind of two-dimension (2D) crystal, composed of monolayers of sp^2 hybridized carbon atoms arranged in a honeycombed network with six-membered rings [14,15]. GNS possesses many advantageous properties, such as excellent electronic conductivity, high surface area and etc. [16–18]. In addition, the theoretical capacity of graphene is of 744 mAh g^{-1} [19,20], twice as large as that of graphite (372 mAh g^{-1}). The incorporation of nanostructured metal oxides into GNS layers will generate a porous network, providing outstanding electron-conducting and ion-transporting pathways [21]. Moreover, the formed metal oxide/GNS nanocomposites may not only reduce the stacking degree of GNS, but also prevent the volume expansion of metal oxides during cycling process. Recently, Co_3O_4/GNS nanocomposites with improved electrochemical performance have been prepared via liquid phase and microwave-assisted methods [22–26]. However, in these composites, Co_3O_4 nanoparticles usually show 0-D structure and tend to aggregate into larger particles during discharge/charge process, which may limit the transportation of ion and/or electron and further affect their reversible lithium storage capacity. On the other hand, the 1-D nanostructure of metal oxides in nanocomposites is more beneficial to expand the gaps between the layers of GNS because of its larger aspect ratio, compared with 0-D nanoparticles. Herein, Co_3O_4 nanorods/GNS nanocomposites have been prepared through a one-spot strategy. Electrochemical performances reveal that the obtained Co_3O_4 nanorods/GNS nanocomposites exhibit improved cycling stability, remarkably high reversible lithium storage capacity and superior rate capability.

2. Experiment

GNS was firstly synthesized by the modified Hummers method as previously reported [27]. In a typical preparation process of Co_3O_4 nanorods/GNS nanocomposites, 0.42 g of $CoSO_4{\cdot}7H_2O$ and 0.9 g of urea were dissolved in 37.5 mL of alcohol–water (1.5:1, v/v) solution. Then 0.3 g of GNS followed by 4 mL of ammonia solution ($NH_3{\cdot}H_2O$, 25%) was slowly added into the above solution. The

* Corresponding author. Tel.: +86 21 54743262; fax: +86 21 54741297.
E-mail address: xfqian@sjtu.edu.cn (X. Qian).

0378-7753/$ – see front matter © 2011 Elsevier B.V. All rights reserved.
doi:10.1016/j.jpowsour.2011.10.131

mixed solution was stirred for 30 min and transferred into a 50 mL Teflon-lined autoclave, sealed and maintained at 120 °C for 12 h. Black precipitates were separated by centrifugation, washed with distilled water and dried in vacuum at 60 °C for over night. Finally, the as-prepared Co_3O_4 nanorods/GNS nanocomposites were further calcined at 450 °C for 3 h under nitrogen flow to remove the residual water molecules and functional groups in the GNS, and to improve the crystallinity of Co_3O_4 in the obtained nanocomposites, which would further improve its electrochemical performance [25]. Pure Co_3O_4 nanoparticles were also prepared by the similar procedure without any GNS.

The morphology and structure of the obtained products were characterized by XRD (Shimadzu XRD-6000, CuKα, 40 kV, 30 mA), FESEM (JSM-7401F) and TEM (JEOL, JEM-2100). Thermogravimetric (TG) analysis was carried out on a Perkin-Elmer 7 instrument to determine the weight ratio of GNS to Co_3O_4. Raman spectra were recorded on a Super LabRam-II spectrometer with a holographic grating of 1800 g mm^{-1}.

The working electrodes were prepared by casting a slurry containing 80% active material (Co_3O_4 nanorods/GNS nanocomposites), 10% acetylene black and 10% polyvinylidene fluoride (PVDF) in a volatile solvent onto a copper foil according to the previous works [21]. Charge–discharge cycles of the cells were evaluated between 0.01 and 3 V vs Li^+/Li using a battery test system (LAND CT2001A model, Wuhan Jinnuo Electronics, Ltd.). All tests were performed at room temperature.

3. Results and discussion

The obtained Co_3O_4 nanorods/GNS nanocomposites were investigated by X-ray diffraction (Fig. 1a), in which curve 1 is the XRD pattern of the obtained nanocomposite after calcination, while curve 2 is that of before calcination. Both the obtained nanocomposites have similar XRD patterns except some differences in the intensity of diffraction peaks, and the main diffraction peaks can be indexed to Co_3O_4 with a face-centered cubic structure (JCPDS CARD No. 42-1467). So the calcinated Co_3O_4 nanorods/GNS nanocomposites are used in the following studies. The additional small and broad diffraction peak appearing at 2θ of 24–27° can be indexed to the disorderedly stacked GNS [26,28], indicating the formation of Co_3O_4 nanorods/GNS nanocomposites. TG analysis indicates that the amount of Co_3O_4 in the Co_3O_4 nanorods/GNS nanocomposites is about 80 wt% (Fig. 1b).

Raman spectroscopy is a non-destructive approach to characterize graphitic materials, in particular to determine the ordered and/or disordered crystal structure of GNS [29]. In the Raman spectrum, the D peak usually corresponds with the *k*-point phonons of A_{1g} symmetry while the G peak is related to the E_{2g} phonons of C_{sp2} atoms [30,31], and their relative intensity gives the clue to the ordered and/or disordered crystal structures of GNS. The Raman spectra of the obtained Co_3O_4 nanorods/GNS nanocomposites and GNS are shown in Fig. 2, a broad D band (1330 cm^{-1}) and a broad G band (1590 cm^{-1}) are observed in both samples [32]. The intensity of the characteristic peak of the D band is slightly stronger than that of the G band, indicating the existence of GNS in the as-prepared nanocomposites.

TEM images were further used to characterize the as-prepared Co_3O_4 nanorods/GNS nanocomposites (Fig. 3). As shown in Fig. 3a, the inconspicuous and sheet-like products can be attributed to GNS because of its thinner structure and lower electron diffraction intensity, and the rod-like products are Co_3O_4 with about 30 nm in diameter and 1–2 μm in length. Furthermore, Co_3O_4 nanorods are disorderly dispersed onto/into the GNS layers to form nanocomposites. The SAED pattern (inset in Fig. 3a) clearly demonstrates the polycrystalline nature of these Co_3O_4 nanorods, implying that

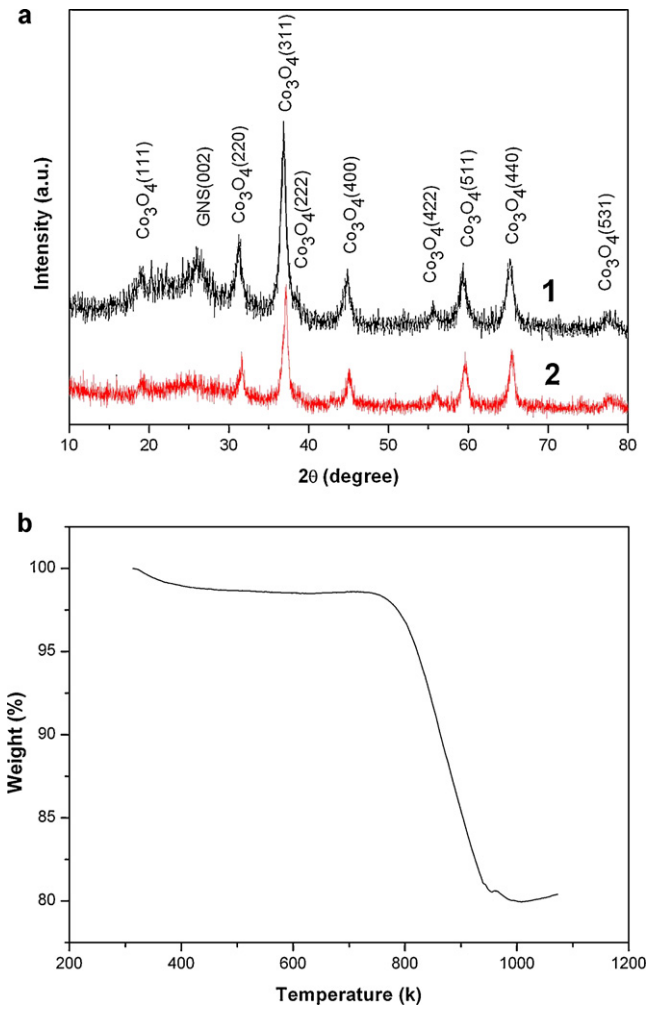

Fig. 1. (a) XRD pattern of the as-synthesized Co_3O_4 nanorods/GNS nanocomposites, (1) after calcination, (2) before calcination. (b) TGA curve of Co_3O_4 nanorods/GNS nanocomposites.

the obtained Co_3O_4 nanorods are composed of primary nanoparticles. The higher magnification image of individual Co_3O_4 nanorod also clearly reveals that it is built by many primary nanoparticles (less than 10 nm). However, only spherical Co_3O_4 nanoparticles are obtained if no GNS exists in the reaction system (Fig. 7a). The above

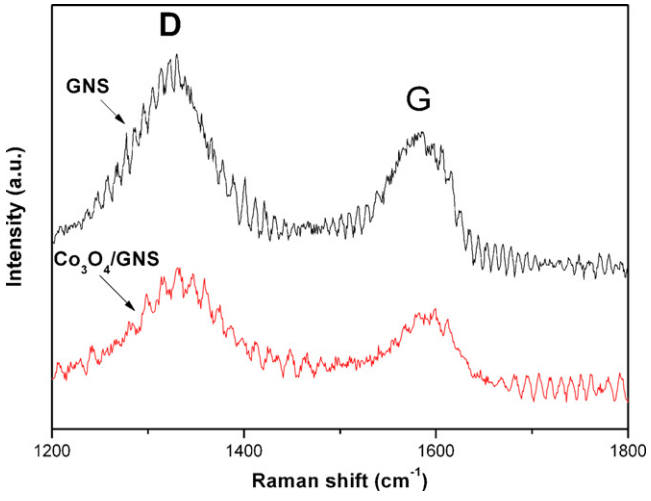

Fig. 2. Raman spectra of Co_3O_4 nanorods/GNS nanocomposites and GNS.

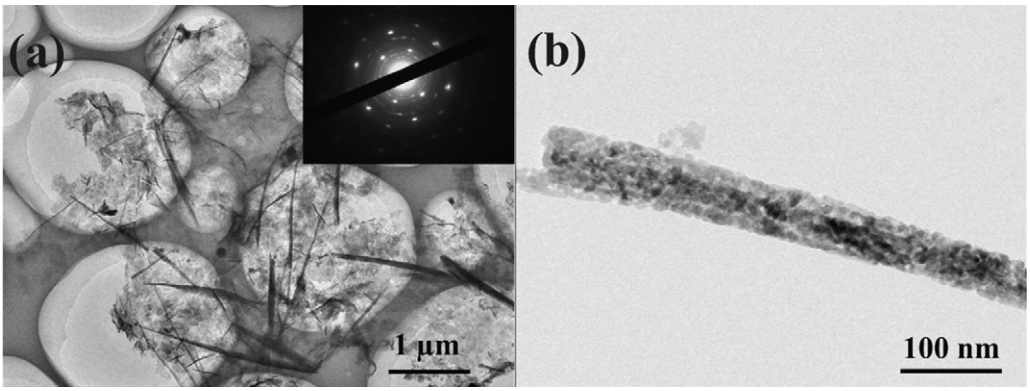

Fig. 3. (a) TEM image of Co_3O_4 nanorods/GNS nanocomposites, the insert in (a) is the SAED pattern. (b) TEM image of individual Co_3O_4 nanorod.

results indicate that the presence of GNS plays an important role in the formation of Co_3O_4 nanorods.

The electrochemical performances of the as-prepared pure Co_3O_4, GNS and Co_3O_4 nanorods/GNS nanocomposites were evaluated. Fig. 4a–c shows the charge/discharge curves at the 1st, 2nd, 10th and 30th cycle of pure Co_3O_4, GNS and Co_3O_4 nanorods/GNS nanocomposites under a current density of 100 mA g^{-1}. As shown in Fig. 4a, the first discharge and charge capacities are 1184 and 854 mAh g^{-1} for pure Co_3O_4, respectively. GNS has a specific capacity of 1014 mAh g^{-1} in the initial discharge step and a reversible capacity of 412 mAh g^{-1} in the first charge step (Fig. 4b). From Fig. 4c, one can see that Co_3O_4 nanorods/GNS nanocomposites have the first discharge and charge capacities of 1303 and 917 mAh g^{-1}, and exhibit much better electrochemical lithium storage performance over pure Co_3O_4 since the 2nd cycle. Furthermore, the obtained Co_3O_4 nanorods/GNS nanocomposites

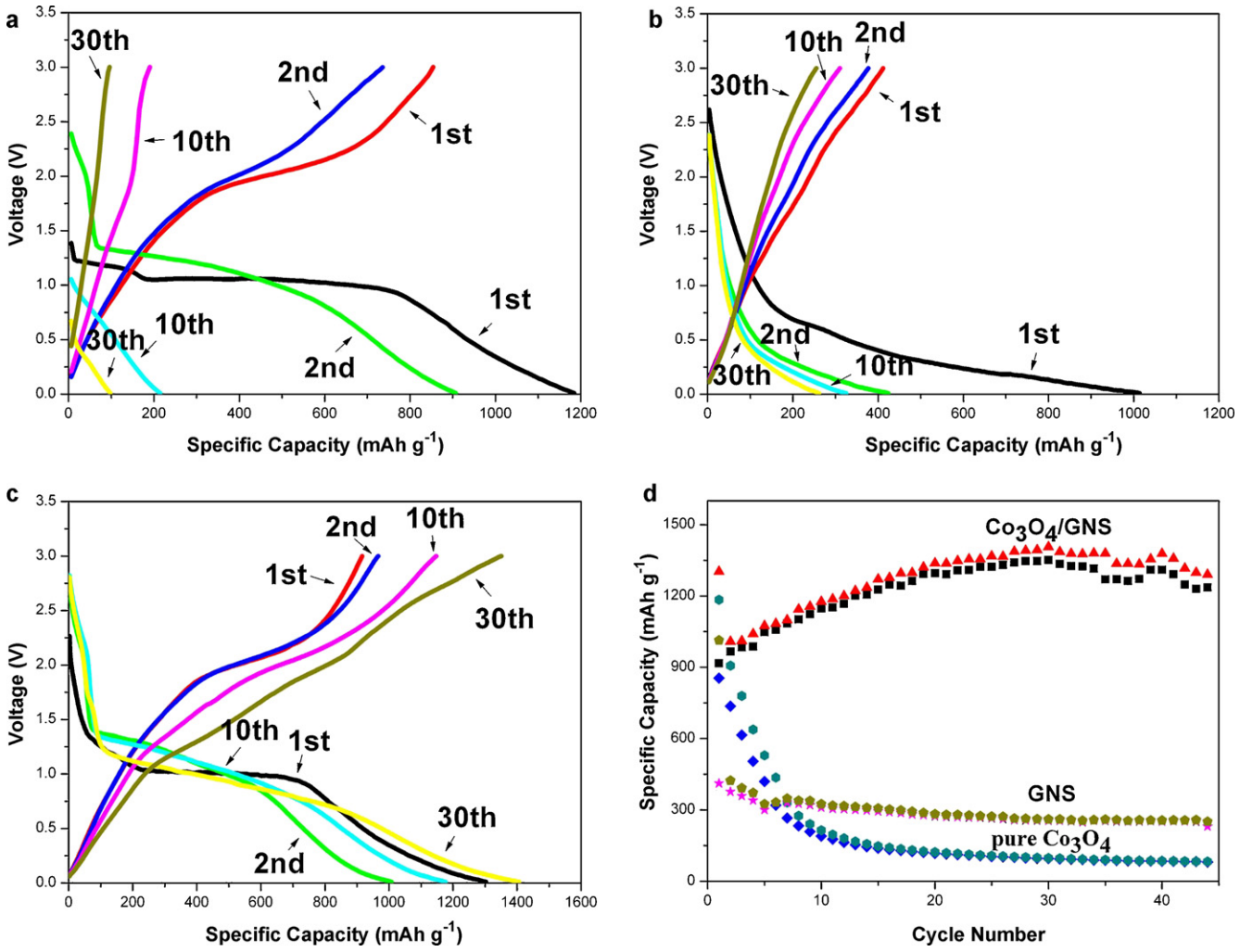

Fig. 4. Typical charge–discharge curves of (a) pure Co_3O_4, (b) GNS and (c) Co_3O_4 nanorods/GNS nanocomposites cycled at the 1st, 2nd, 10th and 30th between 0.01 V and 3.0 V. (d) The comparison of the cycling performance of pure Co_3O_4, GNS and Co_3O_4 nanorods/GNS nanocomposites.

still show a high reversible capacity of ~1150 mAh g^{-1} after ten discharge/charge cycles, and the efficiency rapidly increases from 70.3% in the 1st cycle to 97.5% in the 10th cycle and remains around 97% in the following cycles. While the charge capacity of pure Co_3O_4 drops to 191 mAh g^{-1} with a low efficiency of 88.8% after the 10th cycle. The GNS based electrode (compared with the others) exhibits a lower initial efficiency (only 40.6%) and has no obvious voltage plateau, similar to the previous reports [21,26]. In addition, Co_3O_4 nanorods/GNS nanocomposites show the voltage plateaus around 1.0 V similar to that of pure Co_3O_4. The cyclic performances of all electrodes at a current density of 100 mA g^{-1} are shown in Fig. 4d. Co_3O_4 nanorods/GNS nanocomposites maintain a capacity of 1310 mAh g^{-1} at the 40th cycle, while pure Co_3O_4 electrode only exhibits a poor capacity of 85 mAh g^{-1} after 40 cycles and then almost failing completely. Compared to Co_3O_4 nanorods/GNS nanocomposites, GNS also shows a much worse capacity of 252 mAh g^{-1} at the 40th cycle. More importantly, the reversible capacity of Co_3O_4 nanorods/GNS nanocomposites slightly increases with the increase of cycling numbers and reaches to ~1300 mAh g^{-1} after 40 cycles, which could be attributed to the gradual activation of nanocomposites in the first several cycles. As to unique phenomenon, we believe that the GNS existed in the nanocomposites plays an important role because it can improve the electronic conductivity, decrease the Ohmic loss and further provide the electronic conduction pathway of nanocomposites [21,33]. On the other hand, the 1D structure of Co_3O_4 nanorods can reduce the stacking degree of GNS and further improve the electronic conduction pathway of nanocomposites. As a result, Co_3O_4 nanorods/GNS nanocomposites electrode exhibits much better electrochemical lithium storage performance.

The rate capabilities of Co_3O_4 nanorods/GNS nanocomposites and pure Co_3O_4 electrode are shown in Fig. 5a and b, respectively. It is obvious that Co_3O_4 nanorods/GNS nanocomposites have much better electrochemical performance than that of pure Co_3O_4, and the reversible capacity of Co_3O_4 nanorods/GNS nanocomposites slightly increases with the cycle number increasing. The obtained Co_3O_4 nanorods/GNS nanocomposites keep a reversible capacity of 1104, 1189, 1128 and 1090 mAh g^{-1} at the current density of 100, 200, 500 and 1000 mA g^{-1}, respectively. It can also see that the current density has little impact on the reversible capacity of Co_3O_4 nanorods/GNS nanocomposites. Moreover, the nanocomposites based electrode recovers its original capacity or even a bit higher (the reversible capacity is 1378 mAh g^{-1} for the 45th cycle) when the current density returns to the initial 100 mA g^{-1} after 40 cycles. However, the reversible capacity of pure Co_3O_4 fails quickly at the same conditions, and only 12 mAh g^{-1} for the 40th cycle at 1000 mA g^{-1} is retained, which is much lower than its original capacity (810 mAh g^{-1} at 100 mA g^{-1}). The above results demonstrate that the obtained Co_3O_4 nanorods/GNS nanocomposites show superior rate capability.

As illuminated in Fig. 6, Co_3O_4 nanorods can be deposited onto/into GNS disorderly during the solvothermal process, and they can avoid the aggregation of GNS, which can be also supported by the TEM and SEM images. The high reversible lithium storage capacity, enhanced cycle stability and superior rate capability of the obtained nanocomposites can be attributed to their unique structures and properties of GNS and Co_3O_4 nanorods. First, because of its excellent electronic conductivity, GNS can improve the electronic conductivity of nanocomposites and provide the electronic conduction pathway of nanocomposites during the charge/discharge process, which would reduce the polarization of the electrode and improve its rate capability. Second, the confined effects of GNS nanosheets and the 1D structure

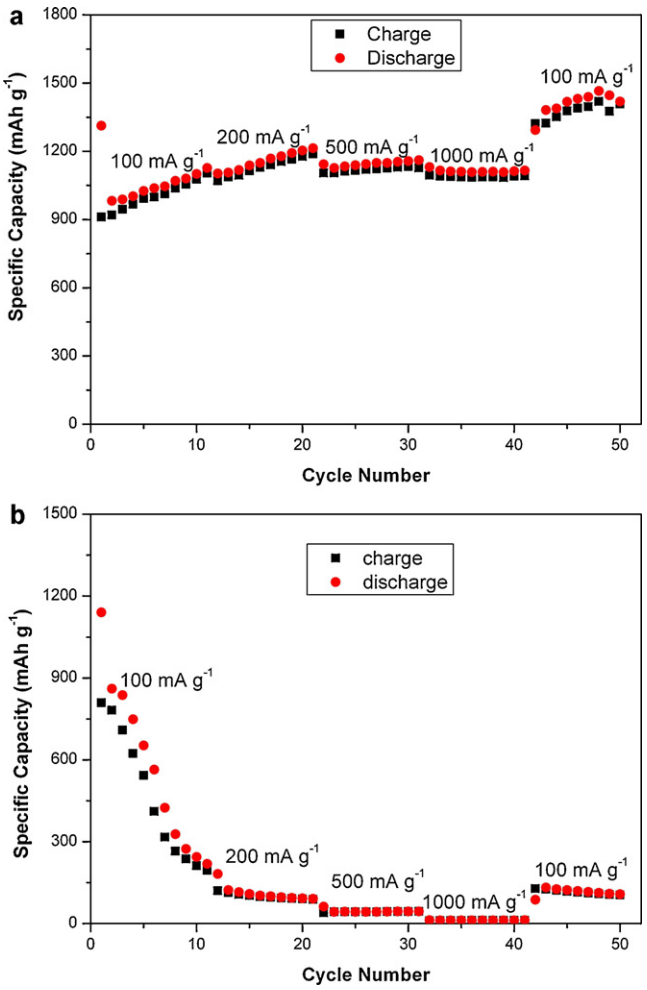

Fig. 5. Rate performance of Co_3O_4 nanorods/GNS nanocomposites (a) and pure Co_3O_4 (b) at various current densities between 100 and 1000 mA g^{-1}.

of Co_3O_4 nanorods in the nanocomposites can avoid the rapid capacity fading because it can block the physical aggregation of Co_3O_4 nanorods during cycling process. Third, the 1D Co_3O_4 nanorods can also reduce the stacking degree of GNS and further improve the electronic conduction pathway of nanocomposites. On the other hand, GNS can serve as a useful mechanical framework for activity materials and improve the stability of electrodes [5,34]. Thus, Co_3O_4 nanorods/GNS nanocomposites with the unique structure could provide fast transport channels for electronic conduction and further improve their electrochemical performances.

In general, metal oxides in their GNS composites are usually in 0-D structures. However, Co_3O_4 nanorods/GNS nanocomposites are obtained in the present works. We believe that GNS plays a key role for the formation of Co_3O_4 nanorods because only spherical Co_3O_4 nanoparticles are prepared without any GNS in the similar reaction conditions (Fig. 7a). From Fig. 7b, one can see that pure GNS is enfolded and stacked with each other similar to a crumpled paper [35]. One can also find that rod-like Co_3O_4 are obtained and dispersed disorderly on the surface of the curly GNS when some of GNS exist in the reaction system (Fig. 7c) and the reaction is carried out in a short reaction time (6 h). However, closer observation reveals that some of spherical Co_3O_4 nanoparticles still exist in the obtained nanocomposites besides nanorods. When the reaction time is further prolonged to 12 h, only Co_3O_4 nanorods are observed in the nanocomposites, and spherical nanoparticles almost disappear (Fig. 7d). These results imply that the Co_3O_4 nanorods are formed

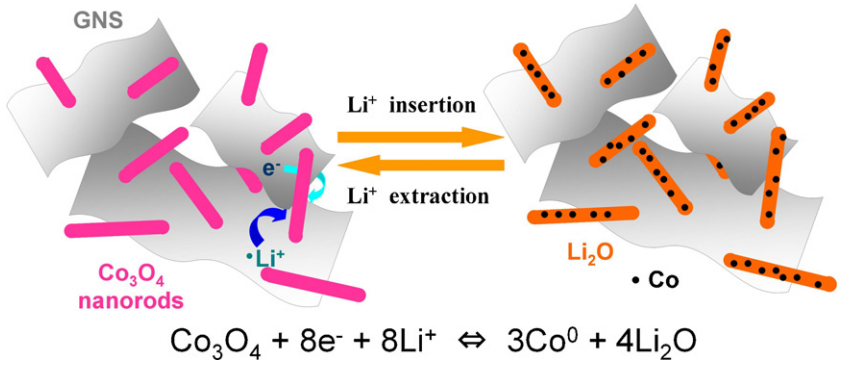

Fig. 6. Schematic illustration of the Co_3O_4 nanorods/GNS nanocomposites before and after the cycling process.

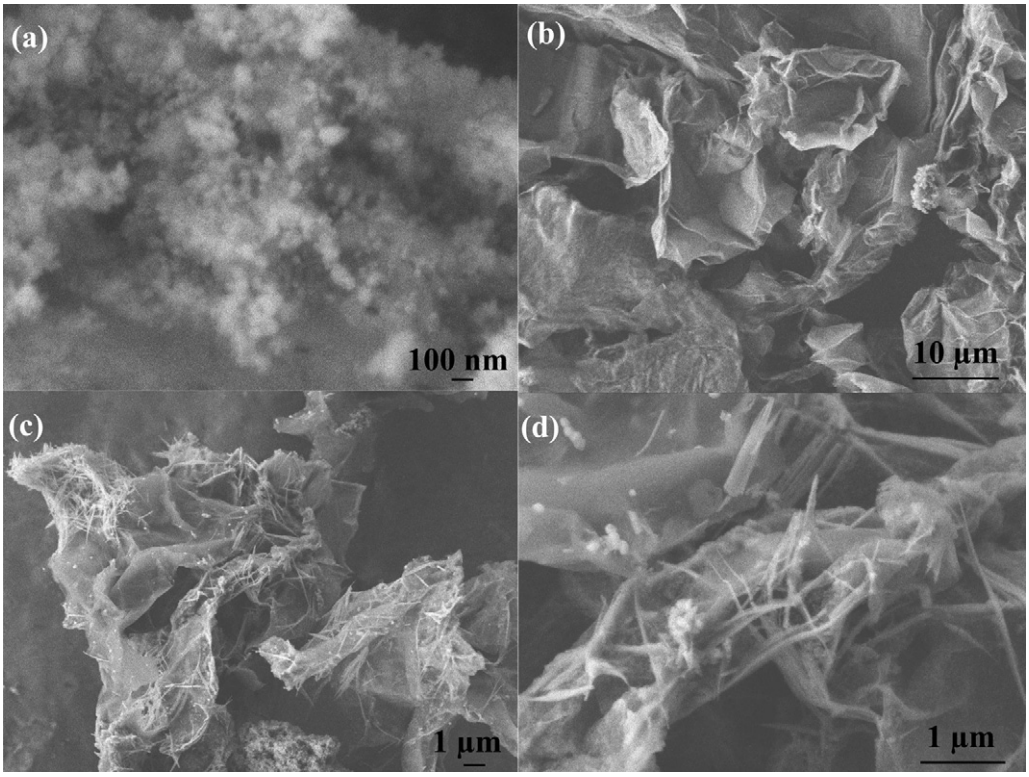

Fig. 7. FESEM images of Co_3O_4 nanoparticle (a), pure GNS (b) and Co_3O_4 nanorods/GNS nanocomposites prepared at solvothermal time for 6 h (c) and 12 h (d).

through the growth or self-assemble of nanoparticles, which is also consistent with the formation of Co_3O_4 nanorods self-assembled from nanoparticles in hydrothermal process [36]. The calcination process will not change the structures of the obtained nanocomposites, and only to remove the residual water molecules and functional groups of GNS. Furthermore, the calcination process can improve the crystallinity of Co_3O_4 in the obtained nanocomposites, which would further improve their electrochemical performances.

4. Conclusions

In summary, Co_3O_4 nanorods/GNS nanocomposites were synthesized by a one-step solvothermal method. Electrochemical performances reveal that the obtained Co_3O_4 nanorods/GNS nanocomposites exhibit improved cycling stability, remarkably high reversible lithium storage capacity and superior rate capability, e.g. approximate 1310 mAh g^{-1} and 1090 mAh g^{-1} of capacity are retained even after 40 cycles at a current density of 100 mA g^{-1} and 1000 mA g^{-1}, respectively. In addition, its reversible capacities and cycling performance are also remarkably improved compared to those of pure Co_3O_4 or GNS. We believe that the improvement of electrochemical performances of Co_3O_4 nanorods/GNS nanocomposites can be attributed to the unique structures and properties of GNS and Co_3O_4 nanorods, which can provide an excellent ion diffusion and electronic conduction pathway, and further lead to a superior electrochemical performance.

Acknowledgments

The work was supported by National Basic Research Program of China (2009CB930400 and 2007CB209705), National Natural Science Foundation of China (21071097 and 20901050), Shanghai Pujiang Program (09PJ1405700) and the key project of State Key Laboratory of High Performance Ceramics and Superfine Microstructure (SKL200901SIC).

References

[1] J. Zhang, L.B. Chen, C.C. Li, T.H. Wang, Appl. Phys. Lett. 93 (2008) 264102.
[2] P.G. Bruce, B. Scrosati, J.M. Tarascon, Angew. Chem. Int. Ed. 47 (2008) 2930–2946.
[3] H.L. Zhang, Y. Zhang, X.G. Zhang, F. Li, C. Liu, J. Tan, H.M. Cheng, Carbon 44 (2006) 2778–2784.
[4] C.C. Li, X.M. Yin, L.B. Chen, Q.H. Li, T.H. Wang, J. Phys. Chem. C 113 (2009) 13438–13442.
[5] M. Zhang, D. Lei, X.M. Yin, L.B. Chen, Q.H. Li, Y.G. Wang, T.H. Wang, J. Mater. Chem. 20 (2010) 5538–5543.
[6] C.Z. Wu, P. Yin, X. Zhu, C.Z. OuYang, Y. Xie, J. Phys. Chem. B 110 (2006) 17806–17812.
[7] Y. Sun, X.Y. Feng, C.H. Chen, J. Power Sources 196 (2011) 784–787.
[8] W.Y. Li, L.N. Xu, J. Chen, Adv. Funct. Mater. 15 (2005) 851–857.
[9] X.H. Huang, J.P. Tu, C.Q. Zhang, F. Zhou, Electrochim. Acta 55 (2010) 8981–8985.
[10] J.Z. Zhao, Z.L. Tao, J. Liang, J. Chen, Cryst. Growth Des. 8 (2008) 2799–2805.
[11] K.X. Wang, M.D. Wei, M.A. Morris, H.S. Zhou, J.D. Holmes, Adv. Mater. 19 (2007) 3016–3020.
[12] J. Yao, X.P. Shen, B. Wang, H.K. Liu, G.X. Wang, Electrochem. Commun. 11 (2009) 1849–1852.
[13] L.F. Cui, J. Shen, F.Y. Cheng, Z.L. Tao, J. Chen, J. Power Sources 196 (2011) 2195–2201.
[14] D. Li, R. Kaner, Science (New York, NY) 320 (2008) 1170–1171.
[15] G. Eda, M. Chhowalla, Adv. Mater. 22 (2010) 2392–2415.
[16] Y.B. Zhang, Y.W. Tan, H.L. Stormer, P. Kim, Nature 438 (2005) 201–204.
[17] M.D. Stoller, S.J. Park, Y.W. Zhu, J. An, R.S. Ruoff, Nano Lett. 8 (2008) 3498–3502.
[18] M. Burghard, H. Klauk, K. Kern, Adv. Mater. 21 (2009) 2586–2600.
[19] J.R. Dahn, T. Zheng, Y.H. Liu, J.S. Xue, Science 270 (1995) 590–593.
[20] Y.H. Liu, J.S. Xue, T. Zheng, J.R. Dahn, Carbon 34 (1996) 193–200.
[21] Y.S. He, D.W. Bai, X.W. Yang, J. Chen, X.Z. Liao, Z.F. Ma, Electrochem. Commun. 12 (2010) 570–573.
[22] S.Q. Chen, Y. Wang, J. Mater. Chem. 20 (2010) 9735–9739.
[23] S.B. Yang, G.L. Cui, S.P. Pang, Q. Cao, U. Kolb, X.L. Feng, J. Maier, K. Müllen, ChemSusChem 3 (2010) 236–239.
[24] G.L. Wang, J.C. Liu, S. Tang, H.Y. Li, D.X. Cao, J. Solid State Electrochem. 15 (2011) 2587–2592.
[25] H. Kim, D.-H. Seo, S.-W. Kim, J. Kim, K. Kang, Carbon 49 (2011) 326–332.
[26] Z.S. Wu, W.C. Ren, L. Wen, L.B. Gao, J.P. Zhao, Z.P. Chen, G.M. Zhou, F. Li, H.M. Cheng, ACS Nano 4 (2010) 3187–3194.
[27] L.H. Tang, Y. Wang, Y.M. Li, H.B. Feng, J. Lu, J.H. Li, Adv. Funct. Mater. 19 (2009) 2782–2789.
[28] G.X. Wang, J. Yang, J. Park, X.L. Gou, B. Wang, H. Liu, J. Yao, J. Phys. Chem. C 112 (2008) 8192–8195.
[29] G.X. Wang, X.P. Shen, J. Yao, J. Park, Carbon 47 (2009) 2049–2053.
[30] A.C. Ferrari, J. Robertson, Phys. Rev. B 61 (2000) 14095–14107.
[31] F. Tuinstra, J.L. Koenig, J. Chem. Phys. 53 (1970) 1126–1130.
[32] S. Stankovich, D.A. Dikin, R.D. Piner, K.A. Kohlhaas, A. Kleinhammes, Y. Jia, Y. Wu, S.B.T. Nguyen, R.S. Ruoff, Carbon 45 (2007) 1558–1565.
[33] S.-M. Paek, E. Yoo, I. Honma, Nano Lett. 9 (2009) 72–75.
[34] J.S. Sakamoto, B. Dunn, J. Electrochem. Soc. 149 (2002) A26–A30.
[35] P. Guo, H.H. Song, X.H. Chen, Electrochem. Commun. 11 (2009) 1320–1324.
[36] G.X. Wang, X.P. Shen, J. Horvat, B. Wang, H. Liu, D. Wexler, J. Yao, J. Phys. Chem. C 113 (2009) 4357–4361.